Chapter 11
Reactive Phase Formation in Thin Films

In this chapter, we will discuss some aspects related to reactive phase formation in thin films. We try to utilize as much as possible the information accumulated during the earlier chapters and built on that. We will first have a brief look on nucleation issues, especially in solid state, before moving into effect of microstructure and impurities on the reactive phase formation. Finally, we will introduce some of the models for phase growth that have been introduced in the past and then discuss in detail about their pros and cons.

The formation of crystalline phases starts by nucleation (which is actually preceded by interdiffusion to create a driving force for the process). The nucleation stage and factors influencing it are discussed in Sect. 11.1. If the stable crystalline phases cannot form directly, metastable structures will form first, as discussed previously in Chap. 1. The formation of amorphous metastable structures is discussed in Sect. 11.2. The kinetics of phase formation is influenced by numerous factors such as impurities, interfaces, and stresses—all these are briefly discussed in Sects. 11.3, 11.4 and 11.5. Finally, growth models developed to describe reactive phase formation in thin films are critically evaluated in Sect. 11.6.

11.1 Role of Nucleation

When a new phase AB is formed at an interface between two elements A and B, the driving force for the reaction is the Gibbs energy of formation of AB from pure A and B. However, the formation of AB involves creation of two new interfaces A/AB and AB/B instead of the old A/B interface. This in general leads into increase in surface energy $\Delta\sigma$ of the system (Fig. 11.1). The classical theory of nucleation mandates that the competition between the gain in free energy ΔG and the energy loss $\Delta\sigma$ should give rise to nucleation mechanisms with an activation energy ΔG^* proportional to $\Delta\sigma^3/\Delta G^2$ (Fig. 11.2). There has been much criticism of the classical theory of nucleation. Nevertheless, it illustrates quite simply the major factors involved in the nucleation process.

A. Paul et al., *Thermodynamics, Diffusion and the Kirkendall Effect in Solids*,
DOI: 10.1007/978-3-319-07461-0_11, © Springer International Publishing Switzerland 2014

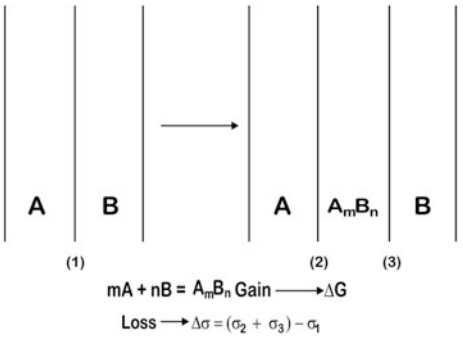

Fig. 11.1 Schematic presentation of the formation of a new phase between A and B

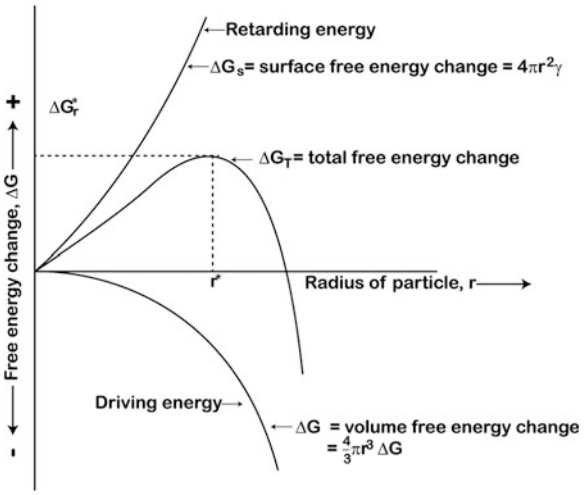

Fig. 11.2 The free energy of a nucleus as a function of its radius, showing the surface contribution (*positive*), the volume contribution (*negative*), and their sum

In its simplest form, classical nucleation theory starts with the equilibrium between two phases of a given substance at either the melting or evaporation point. At the equilibrium point T_c, the free energy change ΔG equals to zero as shown in Chap. 1

$$\Delta G = \Delta H - T_c \Delta S = 0 \tag{11.1}$$

thus leading into

$$\Delta S = \frac{\Delta H}{T_c} \tag{11.2}$$

At the transition temperature, the driving force is zero and nothing can happen. At any temperature T_1 away from the transition temperature, the phase transformation is driven by the driving force

$$\Delta G = \Delta H\left(1 - \frac{T_1}{T_c}\right) \tag{11.3}$$

as long as T_1 is not too far from T_c. This transformation is opposed by the surface energy contribution.

The total free energy of a nucleus with average radius r and free energy ΔG_1 (calculated per unit volume) is expressed generally as

$$\Delta G = br^2\sigma - ar^3\Delta G_1 \tag{11.4}$$

where a and b are geometrical terms taking into account the fact that if the nucleus is crystalline, it will generally not be spherical, because of the anisotropic characteristics of crystalline elements, but tries to adopt some definite shape with minimum surface energy. This can be determined with Wulff construction if sufficient data on surface energies of various crystal planes are available. The relation between the free energy of a nucleus and its radius is shown in Fig. 11.2. As seen, ΔG passes through a maxim that corresponds to the critical size r^* of the nucleus. The population of nuclei smaller than r^* will exist in some form of quasi-equilibrium distribution (e.g., they constantly appear and disappear maintaining some kind of "equilibrium" distribution), whereas nuclei larger than r^* will tend to grow. The value of the critical nucleus can be obtained by derivation of (11.4)

$$r^* = \frac{2b\sigma}{3a}\Delta G_1 \tag{11.5}$$

Furthermore, the free energy of the critical nuclei becomes (at any temperature T) [see, Eqs. 11.3–11.5]

$$\Delta G^* = 4b^3\sigma^3 T_c^2/27a^2\Delta H^2(T - T_c)^2 \tag{11.6}$$

At that temperature, the rate of nucleation ρ^* will be proportional to the concentration of critical nuclei and to the rate at which such nuclei can form, generally some diffusion term of the type $\exp(-Q/kT)$, so that (with a proportionality factor K)

$$\rho^* = K\exp(-\Delta G^*/kT)\exp(-Q/kT) \tag{11.7}$$

Proportionality factor can be explained briefly as follows. Under the dynamic conditions that prevail during nucleation, one expects the number of nuclei of critical size to be less than predicted by thermodynamic equilibrium. This is due to the fact that during nucleation the equilibrium population of critical nuclei is constantly being depleted by the nuclei that grow. The proportionality factor is usually estimated to be about two. It contains also the so-called the Zeldovich factor that is a measure of the probability that fluctuations will cause nuclei, even a size above the critical limit, to dissolve as long as their free energy remains within

kT of ΔG. Thus, every microcluster passing the critical size will not grow. This means also that there is a flat region with a width of δ in the free energy versus radius plot. The Zeldovich factor is the reciprocal of this width. It may assume values of the order of 10^{-2}.

In general in the formation of phases from the end elements, ΔG's are large and thus activation energy (ΔG^*) is small and the nucleation is quite easy. However, after the first phase in the formation of subsequent phases, nucleation may play a decisive role. It should be noted that ΔG^* is actually formed from two parts ΔG^*_1 and ΔG^*_2, $\Delta G^* = \Delta G^*_1 + \Delta G^*_2$, where ΔG^*_1 is related to the density of the crystalline nucleus and ΔG^*_2 to their growth, e.g., diffusion kinetics.

When a nucleus of a new phase is formed, this generally causes a volume change to take place. In solid–solid nucleation, this is accompanied by deformation energy ΔH_d (elastic energy, plus the possible plastic energy). The activation energy for nucleation becomes proportional to $\Delta\sigma^3/(\Delta G_c - \Delta H_d)^2$, where ΔG_c is the "chemical" free energy of bulk phases and the energy associated with deformation is subtracted from that value. One can derive this by first including the term for strain energy into Eq. 11.4. It is also a bit more convenient to consider the free energy per atom of the nucleus rather than the free energy per volume of the nucleus as in Eq. 11.4. The free energy associated with the formation of a nucleus of *n atoms*, Δg, may be written as

$$\Delta g = n\Delta g_C + \eta n^{\frac{2}{3}}\gamma + nh_d \tag{11.8}$$

where

n	number of atoms in nucleus
Δg_C	bulk (chemical) free energy change per atom in nucleus
η	shape factor such that $\eta n^{2/3}$ = surface area
γ	surface tension ≈ surface free energy (exactly for liquids, but only approximately with solids, because in solids there is also another factor (the surface stress) which contributes to surface energy)
h_d	strain energy per atom in nucleus

One may regroup this equation as

$$\Delta g = n(\Delta g_C + h_d) + \eta n^{\frac{2}{3}}\gamma \tag{11.9}$$

The term Δg_C will be negative below the transformation temperature, whereas h_d and γ are both positive. Hence, if $|\Delta g_C| > h_d$, then the first term is negative. The free energy required (Δg^*) to form the critical size nucleus (n^*) is found by differentiating Eq. 11.9 and assuming Δg_C, h_d, η, and γ as constants.

$$\Delta g* = \frac{4}{27}\frac{\eta^3\gamma^3}{(\Delta g_C + h_d)^2} \tag{11.10}$$

A large strain energy h_d reduces the denominator and makes Δg^* large. This means that nucleation is more difficult since the critical size nucleus has a higher energy of formation. This strain energy must be compensated by the lattice and can be done, for example, in silicides, mainly by the diffusive motion of atoms or in metals by dislocation motion. Large strains may change the energetic status of the system and lead to formation of metastable structures (e.g., amorphous phases) as will be discussed later on. It is to be noted that the strain energy is essentially irrelevant to incoherent nucleation. In the case of strained incoherent microcluster, diffusion of thermal vacancies to or from the disordered interface may completely eliminate the strain energy of the system [1]. It is the cases of coherent and semicoherent precipitates where the strain energy becomes relevant. It may be argued that all nuclei are coherent at the very first stages of nucleation. However, at the same time, it should be realized that these phenomena may be inaccessible to experimental methods in many occasions.

The most important parameters determining the phase selection during nucleation are the activation energy of nucleation, Δg^*, the interface energies σ and, the chemical driving force Δg_C, and the elastic strain energy Δh_d—although this last parameter is not relevant to incoherent precipitate cases. In order to evaluate a possible phase selection, reasonable estimates of these parameters must be obtained.

*11.1.1 Activation Energy Δg**

This term can be approximated by the activation energy of diffusion, since the formation of a critical nucleus is mainly determined by diffusional jumps. If this is not available, it can be also approximated with the activation energy of growth of the formed phase in the planar growth regime. From investigations on the later stage of growth, it has been concluded that the precipitates formed in the A/B interface first grow to coalescence within the A/B interface [2]. These results indicate that growth of the nucleus is preferred in the direction of the interface emphasizing the importance of atomic mobility of the A/B interface. Therefore, it is reasonable to assume that the activation energy of volume diffusion is only an upper estimate for the activation energy of growth.

11.1.2 Interfacial Free Energy σ

The interface free energies of crystalline phases consist of two contributions: the chemical contribution related to (chemical) atomic interaction energy, and the structural contribution that originates from the free energy of structural defects associated with semicoherent and incoherent interfaces [3]. The interface free energy terms are hardly known, and even if they are known they are usually bulk

values, and therefore, their use in early stages of phase formation is highly questionable. The interfacial free energies in the solid state are likely to vary between values approaching zero for epitaxial interfaces to maximum values of the order of few J/cm^2 for random interfaces [4]. It should be emphasized that surface free energies of crystalline solids are very much dependent on the history of the specimen, crystal orientation, defect density, impurities etc., and they may depend on the size of the microcluster. Hence, the values of surface free energies for solids are not material constants, but are specific for the sample in question.

11.1.3 (Elastic) Strain Energy Δh_d

Elastic strain energy affects the nucleation, particularly in the case of coherent or semicoherent precipitates, as can be seen from the Eq. 11.10. Here, one will consider only elastic energy, yet the deformations involved can reach proportions beyond the usual elastic limits of the materials. A complete analysis of these effects should take into account the energy stored in plastic deformation as well. The elastic energy resulting from the formation of a third phase will depend on the elastic characteristics of all three phases. In the simplified case where all three phases have the same elastic constants, the energy is given by the following relation [1, 5]

$$\Delta g_{\mathrm{el}} = [2s(1+\nu)/9(1-\nu)]\varepsilon^2 \tag{11.11}$$

where s, the shear modulus of elasticity, is also called the modulus of rigidity, ν is the Poisson ratio, and ε, the strain, is the ratio between the excess volume (under zero stress) and the volume of the hole (here the volume of the reactants) [4]. Ignoring the problems of anisotropy, the following relations from the theory of elasticity can be utilized. Young's modulus E is equal to s times $2(1 + \nu)$; some tables also give the compression or bulk modulus, which is equal to E, divided by $3(1-2\nu)$. The problems of interest here do not concern isotropic materials but three different materials at once. As a zeroth approximation, one may consider that the strain energy is given by an average of the different elastic constants.

11.1.4 The Chemical Driving Force

In order to calculate the chemical driving force for the nucleation of a new phase at the A/B interface, the free energy curves of the solid solution phases and of the formed compounds must be known. These can be determined by applying the CALPHAD method [6–10]. If there exists no information about lattice stabilities and so on in the system, these quantities can be evaluated by ab initio methods. In systems with large negative heat of compound formation, the driving force for the

nucleation of a new phase from the pure elements (with no or negligible terminal solid solubility) is large and approaches to the free energy of compound formation in the reaction temperature. However, in all systems, interdiffusion must occur first to create the necessary driving force for nucleation. Thus, as this may in some cases substantially decrease the initially available driving force for compound formation, this issue must be taken into account [11].

In Thompsons [11] treatment, it is shown that interdiffusion must precede nucleation of new phases and that only after some interdiffusion has occurred there can be a driving force for nucleation (see also Sect. 1.15 for more details). This requirement imposes a kinetic constraint to the first-phase formation. Thus, relative mobilities of diffusing components in competing phases will determine which phase will form first.

In Fig. 11.3, the Gibbs energy curves of the AB system at a given temperature are shown, where A and B have different crystal structures α and β, respectively, and they can form a stable intermediate phase η and a metastable phase M. By assuming that A diffuses into β much faster than B into α, we simplify the case so that only diffusion of A into β needs to be considered. According to the thermodynamic principle of phase equilibrium (see Sect. 1.15), as diffusion proceeds, the first phase to nucleate should be η in β when a sufficient volume of β has reached its equilibrium composition X_{eq} with η (see the tangent line between β and η in Fig. 11.3). Here, it should be remembered from the earlier discussion (Sect. 1.15) that even though η becomes stable at this point, it will not form, since there is no supersaturation, which would provide the necessary driving force for nucleation. If η cannot nucleate, it will become possible for the metastable phase M to nucleate in β when a sufficient volume of β has reached its equilibrium composition X_m with M, provided that the interdiffusion continues. Similar arguments about the required supersaturation as presented above naturally also apply here. The appearance of the metastable phase M would therefore indicate that the time required for nucleation of η is longer than the time required for interdiffusion to the point at which M can nucleate. If neither η nor M can nucleate when the composition of β passes through X_{eq} and X_m sequentially, β will polymorphically transform into M when its composition reaches X_0. This analysis leads to a conclusion that the phase selection depends on the interdiffusion rate in the parent phases as well as the nucleation rates of the product phases.

While the relative rates of nucleation are (ultimately) controlling the phase selection, which phase can nucleate (and grow) is controlled by interdiffusion. Hence, the first-phase formation depends exclusively on the kinetics. It is to be noted, however, that thermodynamics of the system influences the magnitude of the diffusion coefficients via the interaction parameters (see Chap. 1). The nucleation rates are controlled not only by the barriers to nucleation, and hence, the volume Gibbs energy ΔG_v and the energies of the interfaces σ involved, but also by the diffusion required to form critically sized clusters of the product phases. Thompson [11] further suggested that if one component diffused rapidly into the other and self-diffusion of the host was slow, polymorphic phase transitions were favored, so that phases with broad compositional ranges of stability and phases that were rich in

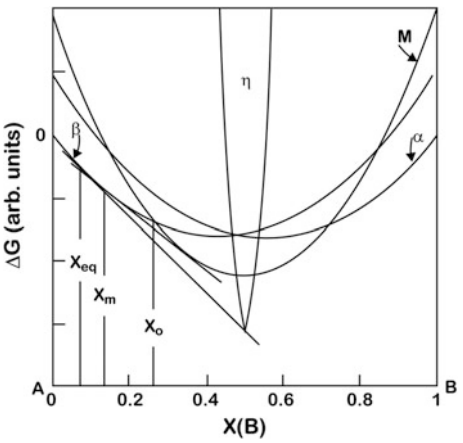

Fig. 11.3 Schematic illustration of the free energy versus composition of a system AB, where elements A and B have different equilibrium crystal structures α and β, respectively, and they can form a crystalline intermetallic phase η and a metastable intermetallic phase M [11]

the slowly moving component were preferred, and such phases with low energy interfaces with the host phase(s) would be especially favored. This points toward amorphous phase formation as will be discussed below.

It should also be emphasized that the free energies of compound formation calculated by the CALPHAD method typically refer to bulk materials. In a small nucleus, the chemical long-range order may not be fully developed due to the interfacial constraints, thus increasing its free energy with respect to the bulk value. In addition, despite the surface energy terms are important in small scales encountered during nucleation, they are typically disregarded in traditional CALPHAD calculations. Further, strain energy may also be important if incoherent interface has not yet been created between the forming nuclei and the matrix. Therefore, the free energy of an ordered chemical compound (as derived from the CALPHAD method) should be viewed as the lower limit for the free energy of the compound nucleus. Thus, the driving force for the formation of a certain compound may be considerably smaller than calculated by using bulk values.

11.1.5 Nucleation Issues in Solid-State Amorphization

The term solid-state amorphization (SSA) is used to describe manufacture of amorphous alloys by solid-state reaction of the crystalline elements. There are two important nucleation-related problems in solid-state amorphization. One is to understand how an amorphous phase forms at an interface between two crystalline elements, the other is to explain how nucleation and growth of a crystalline element is suppressed until an amorphous layer has attained a temperature- and system-dependent critical thickness. The first problem is dealt below and the second in subsequent sections.

The most studied amorphizating system is probably Ni–Zr [12, 13]. It is possible to form amorphous layer between Ni and Zr by annealing in the solid state. Once formed, the layer continues to grow until it has reached a temperature-dependent critical thickness. At this critical thickness the amorphization is terminated by nucleation of the crystalline Ni–Zr compound at the interface between the amorphous alloy and crystalline Zr. Recent experimental investigations have revealed that there is a barrier to nucleation of alloy phases at a Ni/Zr interface and that some Zr grain boundaries are sufficiently potent heterogeneous sites that they reduce this obstacle and allow reaction at a temperature sufficiently low for amorphization to be possible [14–16]. However, calculation based on classical nucleation theory suggests that no such barrier exists [17, 18]. The experimental evidence suggests that either the estimates of the volume and surface terms in the work of Johnson [17] and of Clemens [18] are incorrect or that some additional effects, not included in the classical nucleation analysis, are at work.

As has been discussed above, classical nucleation theory assumes that there is no obstacle for creating small clusters of a new phase within an existing phase. Some of these then acquire critical size and start to grow. Kelton and Greer [19] made a quantitative test based on numerical modeling of the cluster evolution for multistep annealing treatments in lithium disilicate glass. They found the classical theory of nucleation to be valid provided that the critical size was greater than 16 or 20 molecular formula units. The classical approach might not deal adequately with a situation in which the predicted critical size is of molecular dimensions or smaller for two reasons. First, the key parameters in classical theory are the volume free energy and the interfacial free energy as seen above. They may both be functions of cluster size as was discussed earlier. A second, more fundamental problem is that it may be wrong to base nucleation calculations upon clusters of the critical size while neglecting the obstacle to reaction which is presented by creating initial very small clusters of a new phase. This is related to the above treatment of Thompson showing that significant interdiffusion is required before the formation of clusters is possible in systems exhibiting extensive solid solubility.

If classical theory of nucleation is inadequate in circumstances where the predicted critical radius is small, other means of analyzing the initial reaction at, for example, Ni/Zr interface. In particular, one might examine processes, which precedes the formation of clusters of an alloy phase and which could provide a barrier to nucleation, which is larger than the one predicted by classical theory. One could examine first an unmixed interface and then calculate the likelihood of pair's exchanges. As an effect of such exchanges, two solid solutions would form, one of Ni in Zr and one of Zr in Ni. These solid solutions could act as precursors to the glassy phase. The thermodynamic quantities associated with exchange process are assumed to be the molar strain free energy g_s, the molar enthalpy of mixing h_m and the molar configurational entropy s_c [20]. If an interface contains N pairs of atoms, of which a fraction of n have exchanged, the configurational entropy is (as shown in Chap. 1)

$$s_c = -Nk[n\ln(n) + (1-n)\ln(1-n)] \tag{11.12}$$

assuming that the use of Stirling's approximation is justified. Minimizing the free energy of the interface with respect to n gives

$$n = \left[1 + \exp\left(\frac{h + g_s}{kT}\right)\right] \tag{11.13}$$

This expression predicts a barrier to reaction if $(h + g_s)$ is positive.

It is necessary to estimate the magnitudes of h_m and g_s as was done previously in the case of classical approach. Christian [21] suggests that the strain energy that results from dissolving an atom of element B in matrix of element A is

$$g_s = \frac{2s_A K_B (v_A - v_B)^2}{v_B(3K_B + 4s_A)} \tag{11.14}$$

Here, s_A and v_A are the shear modulus and atomic volume of element A, respectively, while K_B and v_B are the bulk modulus and atomic volume of element B. Substitution of atomic volumes from Barret and Massalski [22] and elastic module from Brandes [23] into Eq. 11.14 gives a free energy increase of 1.6×10^{-19} J/atom on dissolving Zr in Ni, and 2.6×10^{-19} on dissolving Ni in Zr. Thus, g_s is 128 kJ/g atom. It must be emphasized that the Eq. 11.14 is only approximate and furthermore, the Ni and Zr lattices will not strain independently of each other, and Ni is likely to dissolve in Zr also interstitially. The large value predicted by Eq. 11.14 is intrinsic to systems with propensities to form glasses by solid-state amorphization (SSA). It has been noticed that disparity between the atomic sizes of species is required in order that an amorphous phase can grow and in order to suppress the nucleation of a crystalline phase(s) as Eq. 11.14 suggests.

An attempt to estimate the enthalpy change h on exchanging a pair of atoms is more complicated because atoms at the unmixed interface already have nearest neighbors, which are not similar. For this reason, only part of the full enthalpy of mixing is available to contribute to h. It is noticeable that even the full enthalpy of mixing -43 kJ/g atom at the equiatomic composition [24] is much less than the evaluated g_s. From these values, it seems that $(h + g_s)$ may be positive and there might be a barrier to exchange atoms at the Ni/Zr interface.

Christian [21] suggests that while single dislocations cannot readily reduce stresses developed in small volumes, larger defects, such as grain boundaries, may be able to. This could explain why grain boundaries at Ni/Zr interfaces are able to act as heterogeneous sites. It does not, however, indicate why Zr, rather than Ni grain boundaries are needed. One reason might be that the free energies associated with certain Zr grain boundaries are greater than the free energies of Ni grain boundaries. A second possibility is that the strain energy associated with dissolving Ni atom in Zr is greater than that caused by dissolving Zr atom in Ni. A third possibility is that the diffusional asymmetry in Ni–Zr makes the slow-diffusing Zr the "matrix" element for SSA, and the reaction must begin in the Zr lattice.

It will be thermodynamically favorable for the precursor solid solutions to transform into an amorphous phase, since the interfacial energy increase associated with the formation of two amorphous/polycrystalline interfaces is probably less than the free energy penalty attributable to strains in the solid solutions. It should be remembered that the incoherent interface can act as a source or sink for thermal vacancies, thus enabling the relief of strains in the system. It is also possible that the stresses developed in the system may change the energetic situation in such a way that amorphous phase becomes more stable than the crystalline ones. The amorphous phase can dissolve solute atoms more easily and is also expected to be able to relax stresses more effectively than crystalline phase. The effect of stresses can be integrated into the Gibbs energy equation of a phase in question. The stress term may lift the Gibbs energy curve of the crystalline phase/phases to such high level that amorphous phase becomes the stable one (see Sect. 1.15).

11.2 Metastable Structures and Nucleation on Concentration Gradient

The types of metastability in alloys have been classified by Turnbull [25] as compositional, structural, and morphological. The degree of metastability is characterized by the free energy excess of the system over that of the equilibrium state. Turnbull [25] expressed this energy per mole as a fraction of $R\bar{T}_m$, where R is the gas constant and $\bar{T}_m$ is the average of the elemental melting points. Compositional metastability is where an equilibrium phase exists outside its normal composition range, and it is associated with large excess energies of up to about $1.0\ R\bar{T}_m$. Structural metastability is where a phase has a non-equilibrium structure, typically with excess energies of about $0.5\ R\bar{T}_m$. Morphological metastability has the lowest excess energy, about $0.1\ R\bar{T}_m$, but is perhaps the most widespread, and generally useful, type of metastability. Its excess energy arises from the abnormally large area of grain boundaries and interphase interfaces.

A system in true metastable equilibrium would not have access to any state of lower free energy by means of a continuous structural change [26]. A good example of such is a fully relaxed amorphous phase, in which any transformation to a lower free energy microstructure can commence only with a discrete nucleation stage which has an energy barrier as discussed. On the other hand, most morphologically metastable microstructures are not in metastable *equilibrium* but can evolve continuously on annealing. In this case, the energy barrier is not nucleation, but the activation energy of atoms making diffusional jumps. Such a system is thermodynamically unstable but is configurationally frozen [26]. Indeed virtually all so-called metastable microstructures, whether in fact metastable or unstable, have technologically useful lifetimes because they are at sufficiently low temperatures to be configurationally frozen. One interesting example of

morphological metastability is the room temperature annealing of either sputter or electrochemically deposited copper in IC fabrication [27–29]. After deposition, the grain size of the films increases after few hours in room temperature. The driving force is provided by the systems tendency to decrease its surface area and thereby its surface energy.

The formation of metastable structures has been observed also in many silicide forming systems [30–34]. The occurrence of these metastable structures is related to the specific features of the thin films. Among these are the very fast atomic transport and very steep concentration gradients often observed in thin-film structures. Since, amorphous films are always metastable, there always exists a crystalline phase or mixture of several crystalline phases, which are thermodynamically more stable than the amorphous phase. In other words, amorphous phases exist only due to some kind of barrier(s), which prevents the formation of equilibrium phases.

In all the above-mentioned silicide systems where the solid-state amorphous (SSA) phase formation has been observed to take place, it has been observed that in the formation temperature range only the smaller atoms are mobile (e.g., Ni in Si and Si in Ta). This can explain the absence of crystalline compound nucleation during the growth of a glassy interlayer [35]. The relative immobility of the larger atom must act as a kinetic constraint to the formation of crystalline compound nuclei. Such nucleation apparently requires the collective motion of both atomic species. Thus, glass growth seems to require diffusional asymmetry in binary diffusion couples. In higher temperatures, the formation of crystalline phases becomes possible due to the enhanced atomic transport.

The absence of compounds in SSA leads to equilibria involving much higher solute contents in the elemental solid solutions that in full equilibrium. The equilibria are also at much lower temperatures than are usual for the phases involved. Figure 11.4 shows the equilibrium phase diagram for Au–Si. This system, in which glass formation by rapid liquid quenching was first found by Klement et al. [36], is a simple eutectic. In binary eutectic systems, the chemical interaction between the elements is repulsive. As the attractive interaction between the elements is increased, compounds will start to appear in a binary system.

A good example of this is Ni–Zr (Fig. 11.5), which exhibits SSA and is indeed one of the most widely investigated systems exhibiting SSA as stated earlier. Since the compounds do not enter into the SSA reaction, the relevant metastable phase diagram is shown by the bold curves in Fig. 11.5. The curves show actually the extended liquiduses. This kind of metastable phase diagrams can be calculated with the help of CALPHAD method as already discussed. Under normal conditions of SSA in Ni–Zr system (composition of the a phase is about $Ni_{60}Zr_{40}$ annealed at 300 °C) [37], it is clear from the metastable phase diagram that there should be eutectic melting of a mixture of the elemental solid solutions. The liquid-like amorphous phase is favored with respect to the solid solutions, and it can therefore be formed by annealing, rather than by rapid quenching as in system like Au–Si. However, the SSA reaction is exothermic and not endothermic as might be expected for melting. This is because the enthalpy of mixing the two

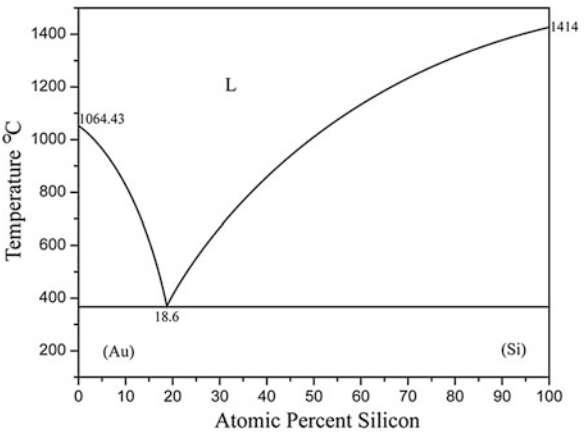

Fig. 11.4 The equilibrium phase diagram of Au–Si, a system showing glass formation by melt quenching, but not by SSA

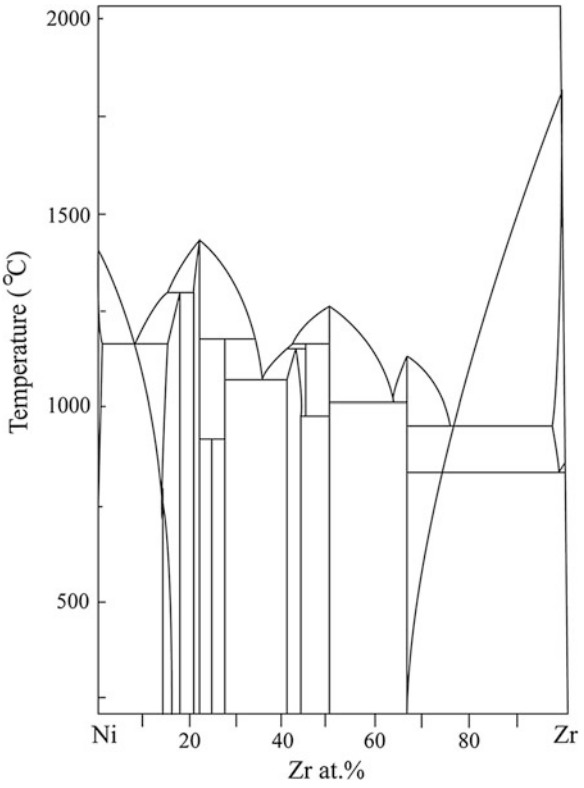

Fig. 11.5 The equilibrium phase diagram of Ni–Zr, a system exhibiting SSA. A possible metastable phase diagram in the absence of compounds is shown by *bold curves* [26]

elements in the liquid-state amorphous phase is highly negative and outweighs the average enthalpy of fusion. Such a negative enthalpy of mixing arises when the liquid alloy has a specific heat significantly higher than the solid state of the

system. In fact, substantial excess specific heats have been measured directly in good glass-forming alloys, for example, $Pd_{40}Ni_{40}P_{20}$ [38]. They are associated with ordering in the liquid state. If there were to be a eutectic melting temperature for Ni–Zr (involving only elemental phases and the liquid), the entropy of melting would have to be positive. Combined with the negative enthalpy of melting, this would imply a negative equilibrium temperature [26]. The conclusion is that for Ni–Zr, the eutectic equilibrium does not exist above absolute zero. Provided that the intermetallic compounds can be avoided, the amorphous phase in the middle of the composition range is stable down to absolute zero. The phase equilibria in systems such as Au–Si and Ni–Zr are related to each other, and an evolution from one type of eutectic system to the other is found as the ordering tendency in the liquid alloy is increased.

One example of impurity-induced amorphous phase formation can be found from the ternary Ta–C–O system. The high-resolution micrograph displayed in Fig. 11.6 reveals the presence of an amorphous layer at the TaC/Cu interface. The composition of the layer was determined to be Ta with marked amounts of oxygen and carbon from the very thin foil (tens of nanometers thick) with the X-ray energy-dispersive spectrometry (EDS) in the analytical TEM. Equally high amounts of oxygen and carbon were not detected from either side of the amorphous layer. The layer is most probably $Ta[O, C]_x$ (i.e., metastable oxide) containing some carbon released from the partly dissociated TaC layer. The formation of the amorphous layer was most likely caused by the presence of oxygen in the films and also because of the diffusion of extra oxygen to the films from the annealing environment. The structure of the Cu overlayer is strongly columnar, thus providing suitable short-circuit paths for oxygen diffusion from the atmosphere during annealing. The overall oxygen content of the as-deposited films is expected to be 1–2 at.%. In particular, the upper part of the TaC layer (i.e., near the TaC/Cu interface) should contain even higher amounts of oxygen. This is owing to the sputtering system, which is equipped with turbodrag pumps to guarantee oil-free deposition, and therefore, the pumping of water vapor from the chamber is not very efficient, although system has load lock. In the case of the Si/Ta/Cu metallization system, secondary ion mass spectrometry (SIMS) analyses revealed an amorphous oxygen-rich layer to be present already in the as-deposited films. Even though this may be the case also in this system, the major part of the incorporated oxygen is most likely present at the grain boundaries of the as-deposited TaC layer.

The isothermal section of the metastable Ta–C–O phase diagram at 600 °C is displayed in Fig. 11.7. The oxygen partial pressure used in the calculations was 0.2×10^{-4} Pa. Since no thermodynamic data for the metastable Ta oxides are available, the data for stable Ta_2O_5 phase are used [39–43]. It is evident that the metastable amorphous $Ta[O, C]_x$ will eventually transform into the stable phases (i.e., Ta_2O_5 and graphite). In fact, according to the XRD results, the formation of Ta_2O_5 took place at 725 °C (Fig. 11.8). When the formation of Ta_2O_5 takes place, TaC and graphite must also be present, since they form a three-phase field in the diagram (Fig. 11.7). TaC phase is expected to come into local equilibrium with metastable $Ta[O, C]_x$ before the formation of stable Ta_2C is possible. Therefore,

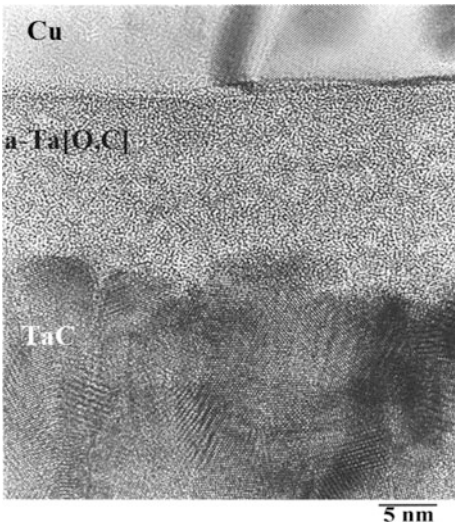

Fig. 11.6 HREM micrograph from the amorphous Ta[O, C]$_x$ phase from the sample annealed at 600 °C for 30 min

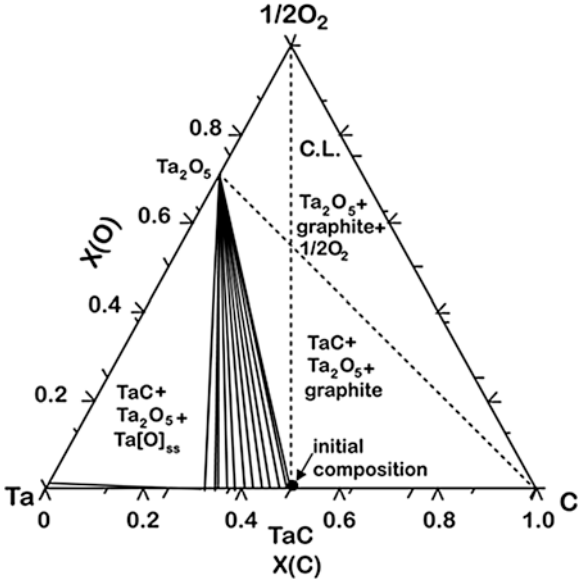

Fig. 11.7 Isothermal section from the evaluated metastable ternary Ta–C–O phase diagram at 600 °C under the external oxygen pressure of about 0.2×10^{-4} Pa. The tie-lines in the TaC–Ta_2O_5 two-phase region are shown in the diagram. The contact line (C.L.) between the TaC film and oxygen indicating the initial unstable equilibrium as well as the approximate composition of the TaC[O] are also shown

the formation of Ta_2C has been suppressed in the calculations to obtain the conditions of the actual metallization structure. The initial state of the system, where the TaC is in equilibrium with the entrapped oxygen, is marked with the contact line (C.L.) in the isothermal section, showing that the situation is highly unstable. The initial composition is located on the contact line and inside the three-phase field (TaC + Ta_2O_5 + graphite) in the isothermal section. Since the overall oxygen content is relatively low ($\sim$1–2 at.%), the composition lies close to the

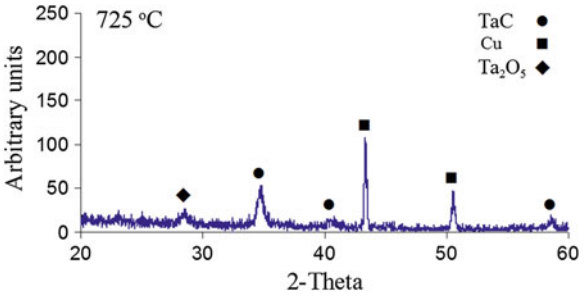

Fig. 11.8 XRD spectra from the Si/TaC(70 nm)/Cu(400 nm) sample annealed at 725 °C for 30 min

Ta–C binary system (the anticipated composition being depicted in Fig. 11.7). When the $TaC[O]_{gb}$ films are annealed at elevated temperatures, oxygen dissolves into the TaC matrix, resulting ultimately in the formation of the stable Ta_2O_5 and graphite. However, owing to the kinetic constraints, the direct formation of the stable tantalum oxide is not possible and the formation of the amorphous $Ta[O, C]_x$ layer takes place. Considering the thickness of the amorphous layer at 600 °C, it is evident that some oxygen has to be incorporated into the films also from the annealing atmosphere. Only after the temperature raises above 700 °C, the relaxation of the kinetic constraints enables the formation of the stable three-phase structure ($TaC + Ta_2O_5 +$ graphite).

The reason for the existence of the $Ta[O, C]_x$ layer in amorphous form at relatively high temperatures is not known. However, what is known, is that metalloids, such as B, C, N, Si, and P, can stabilize amorphous structure in transition metals [44]. It is expected that in this system carbon, which is released from the partially decomposed TaC layer and incorporated into the growing amorphous $Ta[O, C]_x$ layer, stabilizes the amorphous structure. The carbon inhibits the crystallization of the amorphous $Ta[O, C]_x$ up to 725 °C, where the formation of Ta_2O_5 is observed (Fig. 11.8). The reason for the absence of graphite after the crystallization of Ta oxide is the very difficult nucleation of graphite, as observed elsewhere [14]. The stabilizing effect of carbon enables the growth of the amorphous layer to about half the thickness of the original TaC layer at the temperature of crystallization.

The phenomena of SSA have lead to increased interest in interfacial reactions occurring in composition gradients. In fact, as it was stated in the beginning in thin film couples, there often occur very steep concentration gradients. Desré and Yavari attributed the formation of amorphous phase in a thin-film system to a great composition gradient [45, 46]. By using simple thermodynamic arguments, they showed that sharp composition gradients increased the stability of an amorphous phase layer by eliminating or reducing the driving force $\Delta g_{a\to c}$ for nucleation of crystalline intermetallic phases in an amorphous layer. This effect increases with increasingly negative Δh_{mix} and free energy of alloying Δg. As diffusive mixing proceeds further during growth of the amorphous layer, the composition gradient flattened out and the driving force for crystalline phase formation is gradually

restored. The energy barrier for their nucleation also diminishes toward the value of the classic theory

The existence of a composition gradient in the interfacial region has been experimentally observed in the Ni–Si system, and the width of the interfacial region was estimated to be $\leq 2 \times 10^{-3}$ μm [47]. This region can be an amorphous phase or a crystalline solution phase. Figure 11.9b shows the Gibbs energy curve of such an amorphous region (G_{am}) at the A/B interface.

According to the classic theory of homogeneous nucleation, in order for a crystalline stoichiometric phase $\beta - A_{C^*}B_{1-C^*}$ to nucleate in the amorphous region, the nucleus with radius r in Fig. 11.9a must attain a critical radius r^* and equilibrium exists at the interface between the amorphous phase and β. When composition gradient in the amorphous phase is represented by line C(X) as shown in Fig. 11.9a, since the tangents of G_{am} both at C($-r$) and C($+r$) are in touch with the Gibbs energy curve of the β phase, G_β, the nucleus can grow further, which means that the radius r has reached the critical size ($r = r^*$). If the composition gradient in the amorphous phase is greater as represented by C′(X), however, the nucleus will not attain the critical size because the tangents both from C′($-r$) and C′($+r$) miss the tip of G_β. Therefore, there exists a critical composition gradient ∇C_c for β to nucleate. As long as the composition gradient in the amorphous phase is greater than ∇C_c, the crystalline phase will not form. Note also that the orientation and shape of the nuclei with respect to composition gradient are also important as it will change the value of radius.

Following the thermodynamic approach of Cahn and Hilliard for a non-uniform system [48], the Gibbs free energy of a volume v of an amorphous layer can be written as

$$g_a(v) = \rho \int_v [g_0(C) + N_A \chi (\nabla C)^2] dv \tag{11.15}$$

where ρ is the number of moles of atoms per unit volume, g_0(C) is the Gibbs free energy per atom of an amorphous phase with uniform composition C, N_A is Avogadro's number, and χ is a constant. From this can be calculated the Gibbs free energy of formation of a nucleus for the compound $A_{C^*}B_{1-C^*}$ which includes the classic interfacial term

$$\Delta g_N = 24\sigma_{pc} r^2 + 8\rho[\Delta g_{pc}(C*) - N_A \chi (\nabla C)^2] r^3 + {}^4\!/_3 \rho \alpha (\nabla C)^2 r^5 \tag{11.16}$$

where σ_{pc} is the interfacial energy at the polymorphous crystallization front, Δg_{pc}(C*) is the Gibbs free energy of polymorphous crystallization at C*, $\alpha = \partial^2 \Delta g / \partial C^2$ is assumed to be constant in the range $C^* - r\nabla C < C < C^* + r\nabla C$.

As it can be seen from the Eq. 11.16, the concentration gradient leads to a term to the fifth power of the embryo size. As the coefficient of the r^5 is positive, this term will contribute to increase in ΔG_N.

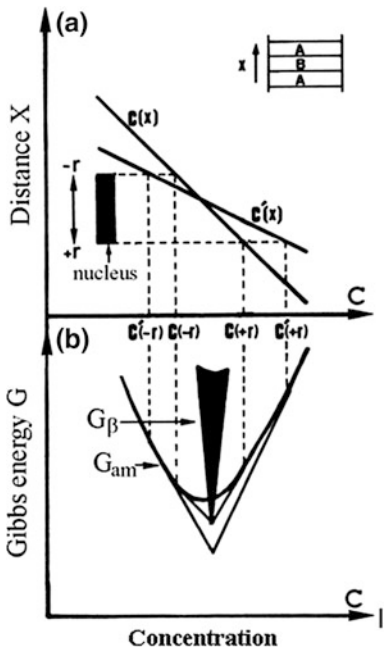

Fig. 11.9 Gibbs energy tangent constructions for compositions at the tips of the critical nucleus of intermetallic phase in an amorphous layer subject to the concentration gradient ∇C [45]

For the typical composition gradients which occur during the solid-state amorphous reaction ($\nabla C \leq 10^{+6}$/cm), the energy factor $N_A \chi (\nabla C)^2$ in Eq. 11.16 is negligible. After some algebra, an analytical expression for the critical gradient ∇C_c, at which Δg_N is both minimum and equal to zero, is obtained as

$$\nabla C_c = \frac{\rho}{9\,\sigma_{pc}} \frac{(2|\Delta g_{pc}|)^{3/2}}{\alpha^{1/2}} \tag{11.17}$$

Above this critical gradient, there is no driving force for compound nucleation.

11.3 Role of the Interfaces

The intrinsic diffusion coefficients of A and B in a given phase are generally different, thus leading into a flux of point defects equal to $J_A - J_B$. This flux changes stepwise at each interface, so that point defects must be created or annihilated at these places. If the interface is unable to perform this task, it leads to the injection of point defects into the substrate [49] (Fig. 11.10). If this injection of point defects into substrate is observed, it is always a signal of some departure from equilibrium, because then the interface is not a perfect sink for point defects as it should be in equilibrium situation. This can lead to the supersaturation or undersaturation of point defects close to interface. Hence, this means that the compound

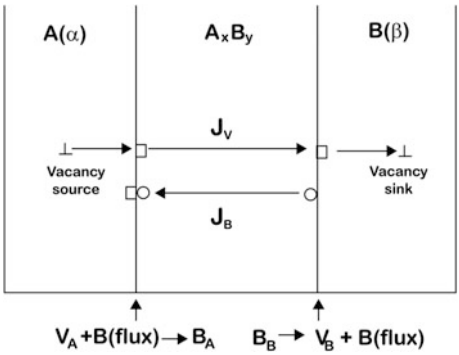

Fig. 11.10 Injection of point defects at the interfaces

will not have the expected composition (non-stoichiometry). It is to be noted that in the Darken treatment of diffusion (see from Sect. 6.7 forward) equilibrium number of point defects are assumed to be present. This means that there should be enough sources and sinks for the point defect to maintain number of vacancies at their equilibrium concentrations. This is typically the case when macroscopic diffusion phenomena are considered. However, when the nanoscale diffusion phenomena are surveyed, the distribution of vacancy sources and sinks may become an issue and the Darken analysis is not valid anymore. Then other type of analyses must be utilized, such as Nazarov-Gurov type approach (see Chap. 5 for more details).

It should also be emphasized that the "chemical constants" (see subsequent sections on the growth models), i.e., reactivity depends on the state of the interfaces and may be changed due to point defect saturation. Interfaces also offer favorable heterogeneous nucleation sites for new phases as they reduce the size of the critical nuclei (see above Sect. 11.1).

11.4 The Role of Grain Boundaries

Thin films possess usually high density of grain boundaries (Fig. 11.11), which can have effect on the growth kinetics. This is because of the enhanced atom transport via the short-circuit paths. A simple situation readily occurs in thin-film experiments: columnar grains, with their long axis along the direction of the diffusion flux. This situation can be modeled by dividing the film into two different parts: one with diffusion coefficient D_{vol} (lattice) and the other with diffusion coefficient D_{gb} (grain boundary). The number of atoms transported per unit area and unit time is given by:

$$M(t) = (A_l J_l + A_{\mathrm{gb}} J_{\mathrm{gb}}) = (A_l D_{\mathrm{vol}} + A_{\mathrm{gb}} D_{\mathrm{gb}}) \frac{dc}{dx} \tag{11.18}$$

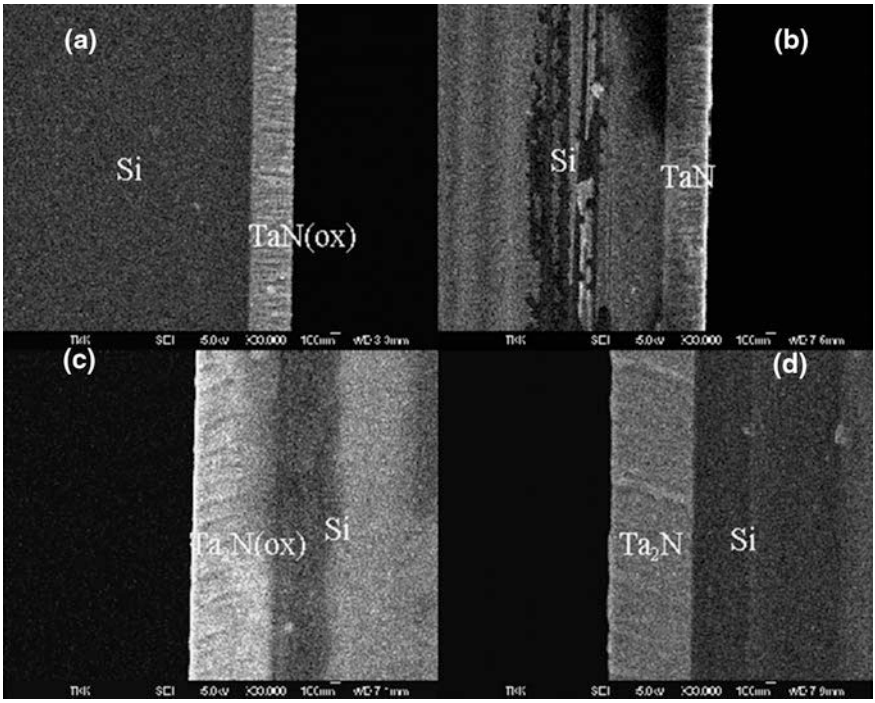

Fig. 11.11 Cross-sectional SEM micrographs of as-deposited. **a** TaN on SiO_2/Si. **b** TaN on silicon. **c** Ta_2N on SiO_2/Si, and **d** Ta_2N on silicon showing columnar microstructure. Micrographs are in the same scale, and scale bar length is 100 nm

where A_l and A_{gb} are the cross sections of the grains and the grain boundaries per unit area.

With conventional thickness δ of grain boundaries, $A_l \approx 1$ and $A_{gb} \approx 2\delta/d$, where d is the average grain diameter [50]. Instead of the lattice diffusion constant D_{vol}, the effective diffusivity D_{tot} must now be considered:

$$D_{tot} = D_{vol} + \frac{2D_{gb}\delta}{d} \tag{11.19}$$

Thus, the value of the diffusion "coefficient" has increased. This may also influence the regime of layer growth, in particular if the thickness of the film is small. Short-circuit diffusion may enhance the atom transport to such an extent that the reaction(s) at the interfaces become rate limiting. More thorough treatment of short-circuit diffusion can be found from Chap. 10.

Grain boundaries also provide favorable sizes for solid-state nucleation, for the same reasons as the interfaces (see section above). Grain boundary nuclei do not necessarily form uniformly over available grain boundary surface (e.g., two grain junction). On the contrary, as it is reasonable to assume that the energy to form a

nucleus of critical size is smaller at grain edges and grain corners (three and four grain junctions, respectively). These sites with lowest critical free energy for formation of nucleus do not necessarily contribute most to the overall nucleation rate. This is because the number of atoms which can participate in the nucleation process also decreases with the dimensionality of the site. Cahn [51] has shown that the opposing effects of lower energy barriers and fewer atoms participating in the nucleation process as the dimensionality of the site can be used to map out different nucleation conditions under which the greatest initial contribution to the nucleation rate is made by the sites of various types.

11.5 Role of the Impurities

Impurities have important effects on the formation of phases in thin film and bulk couples. Presence of some impurity may enhance the formation of a particular phase at the expense of another (see Sect. 11.2 for the case of impurity-induced amorphous phase formation). Impurities may increase or decrease reaction temperatures or influence the kinetics of a phase transformation. Impurities are also frequently responsible for the absence of phases in diffusion couples as compared to the corresponding phase diagram. One example of the increased reaction temperature is the formation of $TaSi_2$, in the reaction between thin Ta film and Si substrate, which occurs at 923 K [52]. However, if there is oxygen at the Si/Ta interface, the temperature of formation will rise well above 1,023 K [53]. Another example of bulk samples is the catalyzing effect of phosphorous on the formation of Cu_3Si in the reaction between bulk copper foil and Si substrate [54]. The effect of impurities on diffusional transport should also be considered. Impurities may segregate preferably to grain boundaries and interfaces. When they segregate to grain boundaries, they may reduce the effect of the short-circuit diffusion paths, thus affecting the mass transport in the system (see Chap. 10 for details).

The driving force for the equilibrium segregation of solute or impurity atoms to grain boundaries is systems tendency to lower its total free energy. In addition to kinetic constraints, the extent of intergranular segregation depends on impurities influence on the grain boundary energy as well as on the factors controlling their solubility, i.e., size factor and chemical interactions between dissimilar atoms. Since both the kinetics and the solubility depend on temperature, the segregation of impurities decreases with increasing temperature. By gathering large amounts of experimental data on grain boundary segregation, Hondros and Seah [55] showed that the smaller the solubility of an impurity in the solvent the higher is its segregation potential. This “rule of thumb” is frequently used when considering the segregation tendency of a given impurity.

The classical free surface adsorption models have often been used for evaluating grain boundary segregation because of the analogies between intergranular segregation and adsorption at free surfaces [56]. This approach is valid if it takes into account the specific features, which differentiate the grain interface from

surfaces. Thus, even the most dilute grain boundary can be regarded as a two-dimensional phase with the same components as in the bulk [57]. These complications imply, among other things, that one has to utilize the extended phase rule instead of the classical phase rule when evaluating the degrees of freedom for the system. A generalized phase rule has been derived for system including surfaces and interfaces by Defay and Prigogine [58]. If c is the number of components, p is the number of 3D phases, φ number of 2D surface phases, and number of degrees of freedom f can be expressed as follows:

$$f + p = (c + 2 - p) - (\varphi - s) = v - (\varphi - s) \tag{11.20}$$

where v is the classical (Gibbs) degrees of freedom (ignoring surfaces) and s is the number of "surface species." Two surfaces are of different species if they separate different couples of bulk phases. For instance, in the case of a grain boundary precipitate β in a matrix α, the interfaces α/α and α/β are of different species and $s = 2$. Also surfaces of different orientations should be considered as different species. It is to be noted that the equilibrium condition, i.e., that the chemical potential of a component i has the same value in all phases of the system, is valid also for grain boundaries and surfaces as shown in Sect. 1.15. Several treatments of intergranular segregation have been published during the past decades. Extensive reviews of the models can be found from Refs. [59, 60].

11.6 Phase Formation in Thin-Film Structures

There has been a view that phase formation in thin-film couples is sequential in comparison to simultaneous phase formation in bulk couples. In many works dealing with formation of silicides, only one or two silicide layers have been reported to grow [52, 59–69]. There have been several different approaches to explain this phenomenon [70–78], which will be summarized briefly next. It is to be noted that the method of evaluating microstructural evolution in diffusion couples introduced in Chap. 8 can be used in thin-film couples and is used as a benchmark when other treatments are discussed. As these phenomena have been thoroughly discussed in that chapter, the treatment is not repeated here for the case of thin-film couples.

11.6.1 Linear-Parabolic Treatment

This treatment has been used by many authors to describe reactive phase formation, including d'Heurle, Gas, and Philibert [49, 68, 69, 74]. The treatment was first used to describe the formation of silicon dioxide [74].

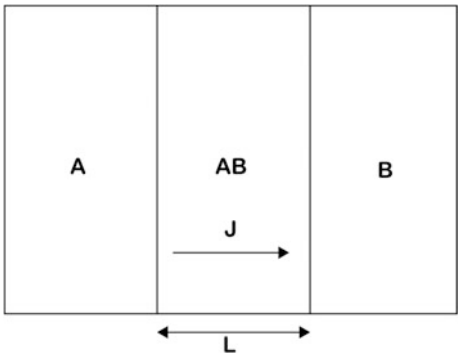

Fig. 11.12 Schematic presentation of the AB growth between the pure elements A and B

11.6.1.1 Growth of One Phase Between Pure A and B

One assumes that a compound AB grows between the pure elements A and B by the diffusion of A atoms (Fig. 11.12). If one starts from the "pure" diffusional growth, one obtains the following equation:

$$J_A = C_A \times M_A \times \frac{d\mu_A}{dL} \tag{11.21}$$

where the mobility is $M_A = \frac{D_A}{kT}$

If one assumes that the intrinsic diffusion coefficient D_A *is not* a function of concentration one obtains

$$J_A = C_A \times \frac{D_A}{kT} \times \frac{\Delta g_A}{L} \tag{11.22}$$

where Δg_A is the *Gibbs energy per A atom* of the reaction A + B = AB. More specifically, it is the required energy to move one mole of A atoms from the A/AB interface across the AB layer to the AB/B interface, i.e., the driving force for diffusion $\Delta\mu_A$. This value can again be obtained from the molar Gibbs energy plot of the system in question using common tangent construction if one has the assessed thermodynamic data of the system available as shown in Sect. 1.15 and in [79, 80]. Since

$$\frac{dL}{dt} = J_A \times v_A \tag{11.23}$$

$$c_A = \frac{1}{v_A} \tag{11.24}$$

then

$$\frac{dL}{dt} = D_A \times \frac{\Delta g_A}{kT} \times \frac{1}{L} \tag{11.25}$$

If one integrates the Eq. 11.25, one obtains the familiar parabolic growth law:

$$L^2 = Kt \tag{11.26}$$

If Eq. 11.26 is considered at very small layer thickness, one encounters a serious problem, since if the L $\approx$ 0, then

$$\frac{dL}{dt} \approx \infty \tag{11.27}$$

This means that pure parabolic kinetics seems impossible. Therefore, d'Heurle et al. [49, 68, 69] introduced the concept of linear-parabolic kinetics.

The starting point is again the Eq. 11.25, where one introduces a "kinetic parameter" to take into account reactions at the interfaces

$$\frac{dL}{dt} = D_A \times \frac{\Delta g_A}{kT} \times \frac{1}{L + K''} \tag{11.28}$$

As the thickness of the layer approaches zero $L \to 0$, then the Eq. 11.28 reaches the form

$$\frac{dL}{dt} \approx D_A \times \frac{\Delta g_A}{kT} \times \frac{1}{K''} \tag{11.29}$$

If one integrates this equation, one obtains:

$$L^2 + K'L = K(t + t_0) \tag{11.30}$$

where $K' = 2\ K''$

When layer thickness grow large and reaction time becomes long (as usually in bulk couples), one obtains the "normal" parabolic growth equation

$$L \to \infty \Rightarrow \quad L^2 \approx Kt \tag{11.31}$$

11.6.1.2 Multiphase Growth Between Pure A and B

If, instead of one phase, several phases grow between A and B, the situation is slightly different, since the growth of a specific phase depends not only its own growth kinetics but also from the growth kinetics of the adjacent phases (Fig. 11.13).Thus, the rate equations are coupled (see Chap. 8 for details). From Fig. 11.13, the following equations can be derived (A is still the only diffusing species)

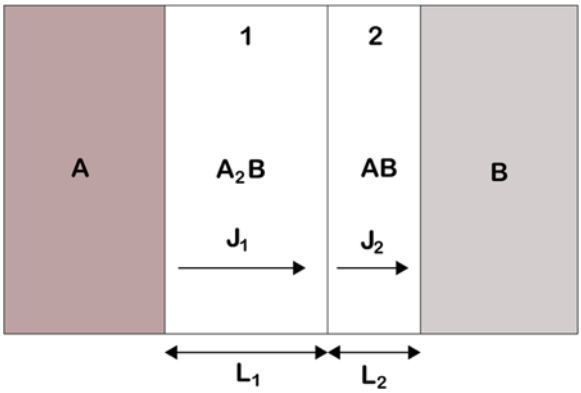

Fig. 11.13 Schematic presentation of multiphase growth between pure elements A and B

$$\frac{dL_1}{dt} \rightarrow J_1 - J_2 \tag{11.32}$$

$$\frac{dL_2}{dt} \rightarrow 2J_2 - J_1 \tag{11.33}$$

where the coefficient 2 in the Eq. 11.33 comes from the stoichiometry.

In layer 1, A atoms diffuse through the A_2B layer to react with the AB layer according to the equation:

$$1. \quad A + AB = A_2B$$

$$\Delta g_1 = \Delta g^f_{A_2B} - \Delta g^f_{AB}$$

In the other layer 2, the growth of AB takes place at two interfaces:

2a.	$A_2B - A = AB$
2b.	$A + B = AB$
total	$A_2B + B = 2AB$
	$\Delta g_2 = 2\Delta g^f_{AB} - \Delta g^f_{A_2B}$

It follows that:

$$\frac{dL_1}{dt} = 2\frac{\alpha_1}{L_1} - \frac{\Omega_1}{\Omega_2}\frac{\alpha_2}{L_2}$$
$$\alpha_1 = D_1\frac{\Delta g_1}{kT} \quad \text{and} \quad \alpha_2 = D_2\frac{\Delta g_2}{kT} \tag{11.34}$$

$$\frac{\Omega_1}{\Omega_2} = \frac{v^{A_2B}}{v^{AB}} \rightarrow \omega \tag{11.35}$$

$$\frac{dL_2}{dt} = 2\frac{\alpha_2}{L_2} - 2\frac{1}{\omega}\frac{\alpha_1}{L_1} \tag{11.36}$$

The layer thicknesses L_1, L_2 and the total thickness $L_1 + L_2$ are functions of $\sqrt{t}$.

If one investigates the growth of different layers:

L_1 grows if the inequality

$$\frac{2\alpha_1}{L_1} > \omega\frac{\alpha_2}{L_2} \tag{11.37}$$

is fulfilled.

Similarly L_2 grows if

$$\frac{\alpha_2}{L_2} > \frac{1}{\omega}\frac{\alpha_1}{L_1}, \quad \text{and} \quad 2\alpha_1 L_2 > \omega\alpha_2 L_1 > \alpha_1 L_2, \tag{11.38}$$

which leads approximately to the equation:

$$2\frac{D_1}{D_2} > \frac{L_1}{L_2} > \frac{D_1}{D_2} \tag{11.39}$$

The ratio $\frac{L_1}{L_2}$ can be solved from the following equation:

$$\frac{L_1}{L_2} = \frac{\frac{2}{\omega}\alpha_1 - \omega\alpha_2 + \sqrt{\left(\frac{2}{\omega}\alpha_1 - \omega\alpha_2\right)^2 + 8\alpha_1\alpha_2}}{4\alpha_2} \tag{11.40}$$

This ratio L_1/L_2 produces to the following diagram where there are three regimes of growth (Fig. 11.14).

At the region M, L_1 grows *and* L_2 shrinks, within the region O, L_2 grows and L_1 shrinks and at the region N, both phases can grow simultaneously. As the time increases and if it is assumed that end elements in reaction couple are not consumed, the reaction couple eventually reaches the N region and both phases can grow simultaneously.

11.6.1.3 "Pure" Diffusional Approach to Multiphase Growth

From the "pure" diffusional point of view regarding the growth of A_2B and AB layers between pure A and B, the following conclusions can be drawn:

(a) *All phases grow simultaneously*. This contradicts experimental results from thin-film experiments where sequential phase formation has been observed
(b) *Growth rate is parabolic*, e.g., $L \rightarrow \sqrt{t}$

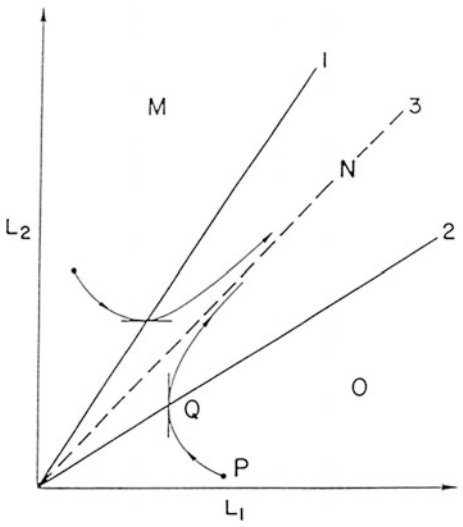

Fig. 11.14 Presentation of the different growth regions in the $A/A_2B/AB/B$ reaction couple under diffusion control [71]

(c) *Phases cannot disappear in reaction couple.* This is as a result of the fact that as the layer thickness goes to zero the growth rate should approach infinity: $L \to 0$ then $\frac{dL}{dt} \propto \infty$

(d) However, even for the pure diffusional growth of the phases, their *thickness ratio is proportional to the ratio of the diffusion coefficients in the layers* $\frac{L_1}{L_2} \to \frac{D_1}{D_2}$

For example, if the ratio of the diffusion coefficients is 10^4, which is of reasonable magnitude for real experiments, and for example, if the layer thickness of the layer 1 is $L_1 = 10^3$ Å, then the thickness of the layer 2 would be $L_2 = 10^{-1}$ Å. In this case, the layer 2 cannot be said to really exist. This shows how within the "pure" diffusional theory, without any further assumptions, one already gets into trouble with layer thicknesses that are readily used in the common thin-film technology. However, this has also been used to defend the traditional "pure" diffusion approach, since it has been stated that all the phases are present in the reaction couple as required, but the thicknesses may be so small that they are impossible to detect.

(e) One can conclude that *with small layer thicknesses with "pure" diffusional theory, mathematics of the theory, and the actual physics are contradictory*

11.6.1.4 Linear-Parabolic Approach to Multiphase Growth

As we noticed, serious problems are encountered with thin-film structures if one uses the traditional "pure" diffusion control approach. On the other hand, if one examines the problem with the help of linear-parabolic growth kinetics the

above-mentioned issues can be avoided. The equations describing the growth of the layers are the following:

$$\frac{dL_1}{dt} = 2\frac{\alpha_1}{L_1 + K_1''} - \omega\frac{\alpha_2}{L_2 + K_2''} \tag{11.41}$$

$$\frac{dL_2}{dt} = 2\frac{\alpha_2}{L_2 + K_2''} - \frac{2}{\omega}\frac{\alpha_1}{L_1 + K_1''} \tag{11.42}$$

If one assumes that the layer formation is sequential as experimentally observed in thin-film experiments, it means that $L_2 = 0$ at the beginning. The driving force for the formation of AB does, however, exist, e.g., $\frac{dL_2}{dt} > 0$, and therefore, the growth rate of AB is positive. Then, one obtains the following inequality:

$$\frac{\alpha_2}{K_2''} > \frac{1}{\omega}\frac{\alpha_1}{L_{1c} + K_1''} \tag{11.43}$$

which leads to the concept of "critical thickness":

$$L_{1c} > \frac{1}{\omega}\frac{\alpha_1}{\alpha_2}K_2'' - K_1'' \tag{11.44}$$

This means that the AB phase will not start to grow until the thickness of the A_2B layer has reached a minimal thickness, *despite the fact that the driving force for the formation of* AB *exists!* Also if the other end element is depleted (A or B) before the A_2B has reached the critical thickness, the AB phase will not occur. Furthermore, if the AB layer is present initially, it will start to shrink as the A_2B layer grows at its expense—if A_2B layer has not yet reached the critical thickness that would enable the simultaneous growth of both phases. If one plots the thickness of the phases similar to the plot as seen in Fig. 11.14, one obtains the same kind of plot—just the nodal lines are translated (Fig. 11.15). The slope of the lines remain unchanged, they are simply translated vertically by the quantity given by the "reaction" factor. There is, however, an additional important feature that can be seen from Fig. 11.15. If the conditions of the growth process lie inside the area marked as R in the figure, the phase 2 (L_2) would disappear under these conditions.

The "simultaneous" phase growth found in the bulk diffusion couples can be explained on the basis of the same critical thickness. In bulk couples, the annealing times are long and the layer thickness are large and therefore the phases "easily" reach the required critical thickness, thus enabling the observation of several phases. It should, however, be emphasized that in the bulk couples also, there are occasions where all the predicted phases are not observed.

Basically, we end up with three rules for the linear-parabolic treatment of two-phase growth

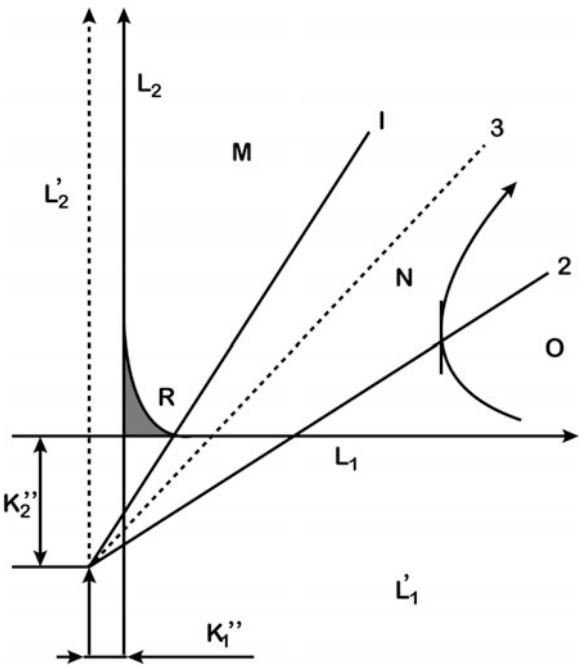

Fig. 11.15 Presentation of the different growth regions in the $A/A_2B/AB/B$ reaction couple according to linear-parabolic kinetics (see text for details) [71]

1. The criterion for the first-phase formation is a kinetic one: It is determined by the value of diffusitivity
2. The first phase grows alone until a critical thickness, which depends on the same parameters, at this point the second phase appears
3. After some transient, the both phases grow simultaneously with proportional thickness increments.

11.6.2 Interfacial Reaction Barrier Approach

The approach was introduced by Gösele and Tu [72, 77] in order to investigate the difference between thin film and bulk reaction couples. It was basically an extension of earlier work by other authors [73–75]. Interfacial reaction barrier was used to describe the energy barrier associated with changes in atomic arrangements or effects due to volume changes at the interface due to the formation of new interface at the expense of the old. In that way, it is somewhat related to interfacial energy.

They used a model system to consider the effect of the interfacial reaction barriers to multiphase growth in a reaction couple where the $A_\beta B$ and $A_\gamma B$ grow between the saturated $A_\alpha B$ and $A_\delta B$ phases ($\alpha > \beta > \gamma > \delta$). It was also assumed

that the $A_\beta B$ and $A_\gamma B$ phases are already present at the beginning with given thickness x_β and x_γ. This assumption was introduced in order to avoid the problems arising from nucleation of the phases. Intention was especially to check whether one of the layers would shrink away completely under various kinetic conditions.

Their model was characterized by the interdiffusion coefficients $\tilde{D}_\beta$ and $\tilde{D}_\gamma$. These coefficients are related to the intrinsic diffusion coefficients by the Darken equation

$$\tilde{D}_\beta = N_B D_\beta^A + N_A D_\beta^B \tag{11.45}$$

The volume of the formed compound Ω_0 per A or B atom is assumed to be constant. They also introduced β which is the ratio of A atoms to B atom in the $A_\beta B$ compound. The shift of the interfaces can be calculated from the equations

$$\frac{dx_\beta}{dt} = G_\beta J_\beta^A - G_{\beta\gamma} J_\gamma^A \tag{11.46}$$

$$\frac{dx_\gamma}{dt} = G_\gamma J_\gamma^A - G_{\gamma\beta} J_\beta^A \tag{11.47}$$

with the (positive) diffusion fluxes of A atoms in the $A_\beta B$ and $A_\gamma B$ layer

$$J_\beta^A = \Delta C_\beta^{eq} k_\beta^{eff} / (1 + x_\beta \kappa_\beta^{eff} / \tilde{D}_\beta) \tag{11.48}$$

$$J_\gamma^A = \Delta C_\gamma^{eq} \kappa_\gamma^{eff} / (1 + x_\gamma \kappa_\gamma^{eff} / \tilde{D}_\gamma) \tag{11.49}$$

where

$$\Delta C_\beta^{eq} = C_{\beta\alpha}^{eq} - C_{\beta\gamma}^{eq} \tag{11.50}$$

and

$$\frac{1}{\kappa_\beta^{eff}} = \frac{1}{\kappa_{\beta\alpha}} + \frac{1}{\kappa_{\beta\gamma}} \tag{11.51}$$

The various quantities with the subscript γ have analogous meaning for the $A_\gamma B$ layer.

The quantities G_β, $G_{\beta\gamma}$, G_γ, and $G_{\gamma\beta}$ take into account the change in composition at the interfaces

$$G_\beta = \Omega_0 (1 + \beta^2) \left(\frac{1}{\alpha - \beta} + \frac{1}{\beta - \gamma} \right) \tag{11.52}$$

$$G_\gamma = \Omega_0 (1 + \beta^2) \left(\frac{1}{\beta - \gamma} + \frac{1}{\gamma - \delta} \right) \tag{11.53}$$

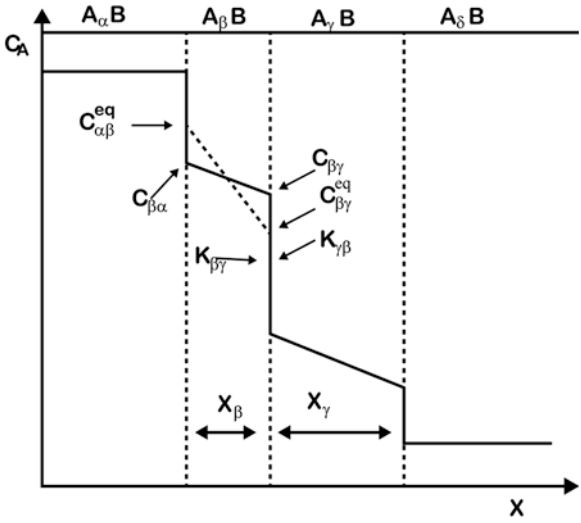

Fig. 11.16 Schematic presentation of the concentration profile of A atoms in the $A_\alpha B/A_\beta B/A_\gamma B/A_\delta B$ diffusion couple

$$G_{\beta\gamma} = G_{\gamma\beta} = \Omega_0(1+\beta)(1+\gamma)/(\beta-\gamma) \tag{11.54}$$

The fluxes described above are assumed to be independent of each other. The schematic presentation of the situation is shown in Fig. 11.16. In the figure, the different parameters are depicted only for the $A_\beta B$ layer, but they are analogous for the other interfaces and layers.

The assumption that the fluxes are independent leads into equations:

$$J_\beta{}^A = \kappa_{\beta\gamma}(C_{\beta\gamma} - C^{eq}_{\beta\gamma}), \text{ at the } A_\beta B \text{ interface} \tag{11.55}$$

and

$$J^A_\gamma = \kappa_{\gamma\beta}(C^{eq}_{\gamma\beta} - C_{\gamma\beta}), \text{ at the } A_\gamma B \text{ interface} \tag{11.56}$$

The quantity $\kappa_{\beta\gamma}$ describes the reaction barrier against the growth of $A_\beta B$ layer at the expense of the $A_\gamma B$ layer, and $\kappa_{\gamma\beta}$ characterizes the reaction barrier against the growth of the $A_\gamma B$ layer at the expense of the $A_\beta B$ layer. The basic difference between this approach and the "traditional" diffusional approach is the occurrence of the interfacial reaction barriers. If the reactions at the interfaces are fast, the reaction barriers tend to approach infinity. Hence, for fast reactions, the growth rates are as described in the "pure" diffusion theory.

The condition for growth of the $A_\beta B$ layer $\frac{dx_\beta}{dt} > 0$ may be expressed in terms of the ratio r of the diffusion fluxes

$$r = \frac{J_{\beta}^{A}}{J_{\gamma}^{A}} \tag{11.57}$$

as

$$r > \frac{G_{\gamma}}{G_{\gamma\beta}} = r_1 \tag{11.58}$$

The analogous condition for the growth of the $A_\gamma B$ layer is

$$r < \frac{G_{\gamma}}{G_{\gamma\beta}} = r_2 \tag{11.59}$$

with

$$r_1 = (1+\gamma)(\alpha-\beta)/(1+\beta)(\alpha-\gamma) \tag{11.60}$$

and

$$r_2 = (1+\gamma)(\beta-\delta)/(1+\beta)(\gamma-\delta) \tag{11.61}$$

where $r_2 > r_1$, holds, since $(\alpha - \beta) < (\alpha - \gamma)$ and $(\beta - \delta) > (\gamma - \delta)$

When the parameters $x_\beta, x_\gamma, D_\beta^i, D_\gamma^i, \kappa_\beta^{\text{eff}}$,and $\kappa_\gamma^{\text{eff}}$have such a values that the flux ratio r is between r_1 and r_2 both layers can grow simultaneously. However, if the flux ratio is not between them, one layer will shrink and the other will grow. Hence, situation is similar as shown already in the Fig. 11.14. This similarity also implies that there should be a critical thickness as in the other two previous treatments. It can be found also within this theory, and it is expressed as follows:

$$x_{\gamma}^{\text{crit}} = \frac{r_1 \Delta C_{\gamma}^{\text{eq}} \tilde{D}_{\gamma}}{\Delta C_{\beta}^{\text{eq}} \kappa_{\beta}^{\text{eff}}} \tag{11.62}$$

where the growth of $A_\beta B$ is reaction controlled and the growth of $A_\gamma B$ diffusion controlled, thus simulating sequential phase formation. It states that the $A_\beta B$ layer cannot coexist with the $A_\gamma B$ layer as long as the thickness of the $A_\gamma B$ layer is below the x_γ^{crit}. This means that even without any nucleation difficulties the $A_\beta B$ cannot form with the $A_\gamma B$ layer in the $A_\alpha B/A_\beta B/A_\gamma B/A_\delta B$ diffusion couple when the thickness of the x_γ is not large enough. This again predicts sequential phase growth.

11.6.3 Similarities Between the Growth Models

It is very interesting to compare the results obtained above and those derived in Chap. 8. Despite the differences between the approaches, all the models lead to similar results. It is also common to both approaches that they neglect the nucleation difficulties in order to avoid complications. In fact, it has been shown by d'Heurle [4] that in most cases nucleation plays a role in the very early stage of the compound formation that is at the present time beyond experimental reach. Nevertheless, nucleation still plays a decisive role with some silicides, especially after the first-phase formation.

In the above two models, reactions at the interface are taken into account with the help of a "chemical constant." This concept is common to both the above models despite the slightly different names that are used. The "chemical constant" is, however, a slightly obscure entity, because it is not clear what are its contents. In Göseles approach [72, 77], it was related to the arrangement of atoms in the interface and the volume changes due to formation of a new interface. Thus, it should contain some "nucleation" contribution also. In the other approach, the meaning of the "chemical constants" was somewhat similar. On the contrary, in the physicochemical approach outlined in Chap. 8 there is no need for *ad hoc* chemical constants as reaction related issues arise naturally from the stoichiometric considerations.

The prediction power of the two models above is quite poor, due to the nature of the "chemical constants." There is no theoretical method at the present to calculate these constants a priori. Hence, they can be determined only by experiments. Also the lack of availability to use measured or estimated thermodynamic and kinetic (diffusion constants) values reduce the use of these approaches. Again, in the physicochemical approach one can readily utilize experimental and theoretical thermodynamic and kinetic data, which makes the approach derived in detail in Chap. 8 a very strong and feasible tool to understand interfacial reaction layer growth in thin film as well as in bulk couples.

From a certain point of view, both of the above models are a posteriori in their nature, as they can explain afterward the phase formation sequence but cannot predict it. Moreover, the "chemical constants" used in all the models are very much case dependent, since they are basically depended on the conditions of the interfaces and are therefore very sensitive to impurities, additional films etc. Furthermore, these constants are not achievable by experimental methods. The approaches, however, fade away the somewhat "traditional" distinction between thin film and bulk couples, since fundamentally the behavior is more or less the same. Nevertheless, in practical situations, the contributions due to the grain boundaries, impurities etc. mentioned above (Sect. 11.5 onwards) must be taken into account in thin films. This does not change the underlying theoretical fact that even in bulk reaction couples phase formation is basically sequential.

If one compares the above treatments to the physicochemical model extensively discussed in Chap. 8, the benefits of the latter over the two approaches are

obvious. As discussed above, the physicochemical model contains only measurable quantities, and it has also predictive power. Thus, it is the opinion of the authors that the physicochemical model should be used whenever the morphological evolution of a binary diffusion zone is rationalized.

References

1. Russel, K.C. *Colloid Interface Sci*., **13**, 205, 1980.
2. Coffey K.R., Clevenger L.A., Barmak K., Rudman D.A., and Thompson C.V., *Appl. Phys. Lett.*, **55**, 852, 1989.
3. Bormann R., *Mat. Res. Soc. Symp. Proc.*, **343**, 169, 1994.
4. d' Heurle F.M., *J. Mater. Res.*, **3**, 167, 1988.
5. Eshelby J.D., *Proc. R. Soc. A London Ser. A.,* **241**, 376, 1957.
6. Saunders N. and. Miodownik A.P, *CALPHAD, Calculation of Phase Diagrams*, Pergammon Materials Series, Elsevier Science, 1998.
7. Kaufman L. and Bernstein H., *Computer Calculation of Phase Diagrams*, Academic Press, New York, 1970.
8. Ansara I., *Pure Appl. Chem.*, **62**, 71, 1990.
9. Lukas H.L., Weiss J., and Henig E.T., *CALPHAD*, **6**, 229, 1982.
10. Bormann R. and Zöltzer K., *phys. stat. sol.(a),* **131**, 691, 1992.
11. Thompson C.V., *J. Mater. Res.*, **7**, 367, 1992.
12. Newcomb S.B. and Tu K.N., *Appl. Phys. Lett.*, **48**, 1436, 1986.
13. Cotts E. J., Meng W.J., and Johnson W.L., *Phys. Rev. Lett.*, **57**, 2295, 1986.
14. Vredenberg A. M, Westendorp J.F.M., Saris F.W., van den Pers N.M., and de Keijser Th. H., *J. Mater. Res.*, **1**, 774, 1986.
15. Meng W.J., Nieh C.W., Ma E., Fultz B., and Johnson W.L., *Mater. Sci. Eng.*, **97**, 87, 1988.
16. Erhart P., Averback R., Hahn H., Yadavalli S., and Flynn C.P., *J. Mater. Res.*, **3**, 1276, 1988.
17. Johnson W.L., Dolgin B., and van Rossum M., in *Glass:Current Issues,* NATO ASI Series, eds. A.F. Wright and L. Dopuy, (Dordrecht:Martinus Nijhoff), 172, 1985.
18. Clemens B.M., *J. Appl. Phys.*, **61**, 4525, 1987.
19. Kelton K.F. and Greer A.L., *J. Phys. Rev. B*, **38**, 10089, 1988.
20. Highmore R.J., *Phil. Mag. B*, **61**, 455, 1990.
21. Christian J.W., *The Theory of Transformations in Metals and Alloys*, Part 1, (Oxford, Pergamon), 1975.
22. Barret C. and Massalski T.B., *The Structure of Metals*, (McGraw-Hill), 1966.
23. Brandes E. editor, *Smithelss Metals Reference Book*, 6th edition (London, Butterworths), 1983.
24. Saunders N. and Miodownik A.P., *J. Mater. Res.*, **1**, 38, 1986.
25. Turnbull D., *Metall. Trans. A*, **12**, 695, 1981.
26. Greer A.L., *Phil. Mag. B*, **61**, 525, 1990.
27. Barmak K., Gungor A., Cabral C., Jr., and Harper J. M. E., *J. Appl. Phys.*, **94**, 1605, 2003.
28. Harper J. M. E., Cabral C., Jr., Andricacos P. C., Gignac L., Noyan I. C., Rodbell K. P., and Hu C. K., *J. Appl. Phys.* **86**, 2516, 1999.
29. Detavernier C., Deduytsche D., Van Meirhaeghe R. L., De Baerdemaeker J., and Dauwe C., *Appl. Phys. Lett.* **82**, 1863, 2003.
30. Herd S., Tu K.N., and Ahn K.Y., *Appl. Phys. Lett.*, **42**, 597, 1983.
31. d'Heurle F.M., Petersson C.S., Baglin J.E.E., La Placa S.J., and Wong C.Y., *J. Appl. Phys*., **55**, 4208, 1984.
32. Vanderwalker D.M., *Appl. Phys. Lett.*, **48**, 707, 1986.
33. Holloway K. and Sinclair R., *J. Appl. Phys.*, **61**, 1359, 1987.

34. Meyerheim H.L., Lengeler B., and Göbel H.E., *J. Appl. Phys.*, **68**, 2694, 1990.
35. W.L. Johnson, Prog. *Mater. Sci.*, **30**, 1986, 81.
36. W. Klement, R.H. Willens, and P. Duwez, *Nature*, **187**, 1960, 869.
37. Clemens B.M., Johnson W.L., and Schwarz R.B., *J. Non-Crystal. Solids*, **61**-**62**, 817, 1984.
38. Evans P.V., Garcia-Escorial A., Donovan P.E., and Greer A.L., *MRS Symposium Proceedings*, **57**, 234, 1987.
39. E. Gebhardt and H. D. Sehezzi, Z. Metallkd., **50**, 521, (1952).
40. H. Jehn and E. Olzi, *J. Less-Common Met.*, **27**, 297, (1972).
41. S. Stecura, *Metall. Trans.*, **5**, 1337, (1974).
42. R. Lauf and C. Altstetter, *Scr. Metall.*, **11**, 938, (1977).
43. G. Boreau and P. Gerdanian, *J. Phys. Chem. Solids*, **42**, 749, (1981).
44. M.A. Nicolet, in: *Diffusion in Amorphous Materials,* eds. H. Jain and D. Gupta, (TMS Warrendale, 1994), pp. 225-234.
45. Desre P.J. and Yavari A.R., *Phys. Rev. Lett.*, **64**, 1533, 1990.
46. Desre P.J., *Acta Metall. Mater.*, **39**, 2309, 1991.
47. Grunthaner P. J., Grunthaner F. J., and Mayer J. W., *J. Vac. Sci. Technol*, **17**, 924, 1980.
48. Cahn W. and Hilliard J. E., *J. Chem. Phys*, **28**, 258, 1958.
49. Philibert *J., Appl. Surf. Sci.*, **53**, 74, 1991.
50. Kaur I. and Gust W., *Fundamentals of Grain and Interphase Boundary Diffusion*, Ziegler Press, 1989.
51. Cahn J.W., *Acta Metall.*, **4**, 449, (1956).
52. Ottaviani G., *Thin Solid Films*, **140**, 3, 1986.
53. Christou A. and Day H.M., *J. Electr. Mater.*, **5**, 1, 1976.
54. Becht J.G.M., "The Influence of Phosphorous on the Solid State Reaction Between Copper and Silicon or Germanium", Doctoral Thesis, Tech. University of Eindhoven Netherlands, 1987.
55. Hondros E. and Seah M., *Int. Met. Rev*, **22**, 262, 1977.
56. Hondros E. and Seah M., *Metall. Trans. A*, **8A**, 1363, 1977.
57. Guttmann M., *Metall. Trans. A*, **8A**, 1383, 1977.
58. Poate J.M. and Tisone T.S., *Appl. Phys. Lett.*, **24**, 391, 1974.
59. Lau S.S., Mayer J.W., and Tu K.N., *J. Appl. Phys.*, **49**, 4005, 1978.
60. van Gurp G.J., van der Weg W.F., and Sigurd D., *J. Appl. Phys.*, **49**, 4011, 1978.
61. Scott D.M. and Nicolet M.-A., *Phys. Stat. Solidi.*, **66**, 773, 1981.
62. Tsaur B.Y., Lau S.S., Mayer J.W., and Nicolet M.-A., *Appl. Phys. Lett.*, **38**, 922, 1981.
63. Eizenberg M. and Tu K.N., *J. Appl. Phys.*, **53**, 6885, 1982.
64. Petersson C.S., Baglin J.E.E., Dempsey J.J., d'Heurle F.M. and La Place S.S., *J. Appl. Phys.*, **53**, 4866, 1982.
65. Canali C., Catellani F., Ottaviani G. and Prudenziati M., *Appl. Phys. Lett.*, **33**, 187, 1978.
66. Coulman B. and Chen H., *J. Appl. Phys.*, **59**, 3467, 1986.
67. Lien C.-D., Nicolet M.-A., and Lau S.S., *Thin Solid Films*, **143**, 63, 1986.
68. d'Heurle F.M. and Petersson C.S., *Thin Solid Films*, **128**, 283, 1985.
69. Gas P. and d'Heurle F.M., *App. Surf. Sci.*,**73**, 153, 1993.
70. Philibert J., *Materials Science Forum*, **155**-**156**, 15, 1994.
71. d' Heurle F.M., "The Kinetics of Reactive Phase Formation: Silicides", in *Silicides: Fundamentals and Applications*, (Eds. L. Miglio and F. d'Heurle), World Scientific, pp. 169-186, 2001.
72. Gösele U. and Tu, K. N. *J. Appl. Phys.*, **66**, 2619, 1989.
73. Geguzin Ye Ya, Kaganovskiy Yu.S, Paritskaya L.M., and., Solunskiy V.I, *Phys. Met. Metallogr.*, **47**, 127, 1980.
74. Deal E. and Grove A.S., *J. Appl. Phys.*, **36**, 3770, 1965.
75. Farrel P., Gilmer G.H., and Suenaga M., *Thin Solid Films*, **25**, 253, 1975.
76. Taguchi O., Iijima Y., and Hirano K., *J. Japan Inst. Metals.*, **51**, 4, 292, 1987.

77. Gösele U. and Tu K.N., *J. Appl. Phys.*, **53**, 3252, 1982.
78. Wagner C., *Acta Metall.*, **17**, 99, 1969.
79. Gulpen J., "Reactive Phase Formation in the Ni-Si System", Doctoral Thesis, Technical University of Eindhoven, The Netherlands, 1995.
80. Rönkä K., "Time-Dependent Microstructural and Compositional Changes at the Interfaces between Materials in Electronics", Doctoral Thesis, Helsinki University of Technology, Finland, 2001.